DYNAMIC DUCTILE FRACTURE OF ALUMINUM SEN SPECIMENS AN EXPERIMENTAL-NUMERICAL ANALYSIS

Jonghee Lee, Matthew T. Kokaly and Albert S. Kobayashi
University of Washington
Department of Mechanical Engineering
Seattle, Washington 98195-2600, USA

ABSTRACT

A hybrid experimental-numerical analysis was used to study the dynamic fracture parameters which may control rapid fracture of ductile materials, i.e. 7075-T6 and 2024-T3 aluminum alloy, single edge notched (SEN) specimens of 1.6 mm thickness. The transient displacement field surrounding a rapidly propagating crack was recorded by Moiré interferometry and together with the crack extension history, was used to drive a dynamic elasto-plastic finite element (FE) model of the fracturing SEN specimens. The measured and computed crack tip opening angles (CTOA) coincided and remained constant during crack propagation. The far- and near-field J's increased and vanished, respectively but the T^*_ε remained constant with crack propagation. Thus the T^*_ε/CTOA criteria proposed for stable crack growth could be the necessary condition for rapid crack propagation in these thin aluminum specimens.

KEYWORD

Dynamic fracture, aluminum, Moiré interferometry, dynamic finite element analysis, J-integral, T^*_ε-integral, crack tip opening angle (CTOA).

INTRODUCTION

While dynamic fracture in the presence of small scale yielding has been amply characterized by dynamic fracture toughness, K_{ID}, no comparable fracture parameter has been identified for dynamic fracture in the presence of large scale yielding. The J-integral, which is widely used to identify the onset of ductile fracture, loses its path independency with crack extension due to the large scale unloading in the trailing wake of the propagating crack. In addition, the near-field J-integral has been shown to vanish after reaching a peak value at the initiation of crack extension and thus cannot be used as a characteristic crack-tip parameter. The resultant inadequacy of the ASTM procedure for determining the J resistance curve for stable crack growth with a trailing unloaded region has been documented by May and Kobayashi (1995). However, the inertia effect associated with dynamic ductile crack propagation, which will exasperate this condition, has not been studied.

On the other hand, Brust et al (1985, 1986) showed that the T^*_ε-integral, which is based on the incremental theory of plasticity, reaches a steady state value under stable crack growth and unloading and thus could be an effective dynamic ductile fracture criterion. In this integral, the unloading effect is accounted by stretching the contour of T^*_ε with the extending crack tip and

computing the energy inflow into the wake as well as the frontal crack tip region. In contrast, the J-integral only computes the energy in flow in a closed contour which moves with the crack tip. Like the J-integral, the T^*_ε is also a path dependent integral in the presence of large scale yielding and unloading. Thus it must be evaluated near the crack tip if it is to be considered a crack tip parameter. This near-field T^*_ε, as defined by Stonesifer and Atluri (1982) in terms of incremental plasticity is:

$$\Delta T^*_\varepsilon = \int_{\Gamma_\varepsilon} \left[\Delta W \cdot n_1 - (t_i + \Delta t_i) \cdot \Delta u_{i,1} - \Delta t_i \cdot u_{i,1} \right] ds \qquad (1)$$

where W is the work density and t_i and u_i are the traction and displacement, respectively. Γ_ε is the contour of line integration very close to crack tip and unlike the J-integral contour, which moves together with the crack tip, remains stationary. The fundamental difference between the J and T^*_ε-integrals are that the former, which is based on deformation theory of plasticity, neglects the unloading effect in the wake of the extending crack while the latter accounts for this effect.

As for experimental dynamic ductile fracture studies, Kobayashi et al (1967a, 1967b) used a single frame, ultra-high speed photography and geometric Moiré to show that the transient strain fields in fracturing magnesium, 7075-T6 and 7178-T6 aluminum alloy, central-notched (CN) specimens varied with $1/r^{(1/2)}$ while the corresponding static strain varied with a higher singularity. These results suggested that under dynamic condition, the propagating ductile crack can be modeled by dynamic linear elastic fracture mechanics (LEFM) and thus justified the earlier and extensive LEFM approach to dynamic fracture which is documented by Kanninen and Popelar (1985). This pseudo-elastic response was associated with a relatively high crack velocity of 10 to 20 percent of the Rayleigh wave velocity generated by an over-driven crack propagating from a blunt notch. In contrast, most dynamic ductile fractures are associated with a lower crack velocity or the transition region between stable and rapid crack growth, say at a crack velocity of 5 to 10 percent of the Rayleigh wave velocity. This paper explores the dynamic ductile fracture associated with a crack propagating at this pseudo-dynamic velocity.

METHOD OF APPROACH

Moiré interferometry was used to determine the transient displacement field perpendicular to the running crack in 2024-T3 and 7075-T6 aluminum alloy, SEN specimens. The missing displacement field parallel to the crack was computed through the use of a hybrid experimental-numerical analysis where the measured transient displacement field together with the crack propagation history were used to drive a dynamic, elasto-plastic FE model of the SEN specimen. The complete displacement field was then used to extract fracture parameter(s), such as J and T^*_ε-integrals, and CTOA, which could control the running ductile crack.

EXPERIMENTAL PROCEDURE

A new Moiré interferometry technique by Wang et al (1994), which combines the advantages of geometric Moiré and traditional Moiré interferometry, was used to measure the large strains in the vicinity of the running crack tip. The method uses a steep grating of low-spatial frequency, i.e. 40 lines/mm in this study, on a mirror finished specimen surface to achieve high contrast Moiré fringes on the specimen surface. Four frames of the Moiré fringe patterns corresponding to the dominant vertical displacements were recorded by an IMACON 790 camera. This limited number of frames and the fixed framing rate, i.e. 10,000 frames per second, required multiple recordings of identically loaded SEN specimens at different delay timings in order to capture the entire fracture event which lasted about 1.2 milliseconds. Despite all efforts to generate reproducible tests, no two dynamic fracture tests are identical

and thus the final composition was made with the consideration of the load-time history and the varying crack opening profile of each fracture event.

Figure 1 shows the SEN specimen and Fig. 2 shows the static uniaxial stress versus strain relations for the 2024-T3 and 7075-T6 aluminum plates used. The latter was obtained by averaging the uniaxial stress-strain data in the direction parallel and perpendicular to the rolling direction. The use of static stress-strain relations were justified since the estimated maximum strain rate during the dynamic fracture event was only 539 sec^{-1}. For the elasto-plastic FE analysis, the following power hardening relations were fitted to the experimentally determined stress-strain relations.

$$\frac{\varepsilon}{\varepsilon_o} = \frac{\sigma}{\sigma_o} + \alpha \left[\frac{\sigma}{\sigma_o} \right]^n \qquad (2)$$

where σ_o is a reference yield stress and $\varepsilon_o = \frac{\sigma_o}{E}$ is the associated elastic strain, and α and n are the material constants. The two coefficients, α and n, for the power hardening relation for each aluminum are listed next to their respective stress-strain curves in Fig. 2.

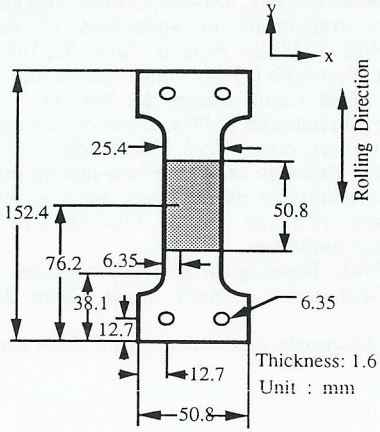

Fig. 1. Aluminum SEN specimen.

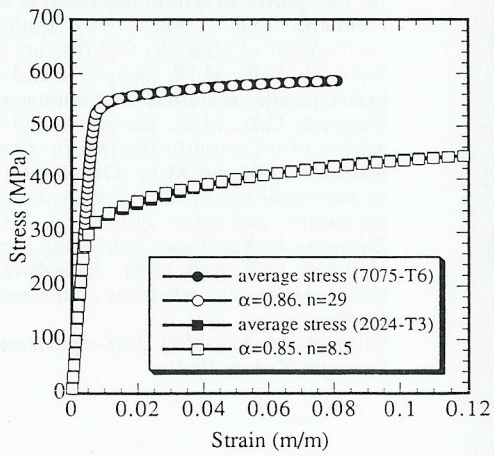

Fig. 2. Uniaxial stress-strain relations of aluminum.

The J and T^*_ε evaluation procedures developed for numerical analysis, as described in the following section, were used to evaluate J and T^*_ε based on the Moiré fringe data.

NUMERICAL PROCEDURE

The FE model consisted of a truncated SEN specimen where the measured vertical displacement together with an assumed vanishing tangential surface traction were prescribed on a horizontal cross section, 10 mm from the crack. Symmetry about the crack was assumed and therefore only half of the specimen was modeled. This FE model of the truncated SEN specimen consisted of graded finite elements with the smallest element being 0.25 mm square along the crack. A

dynamic elasto-plastic FE analysis was conducted by driving the FE model with the measured time-varying displacement boundary condition and the crack tip location.

The FE results were then used to compute the J and T^*_ε-integral values following the procedure developed by Okada and Atluri (1996). The algorithm for dynamic J computation was programmed since the dynamic elasto-plastic FE code used in this study (ABAQUS Version 5.4-1) did not contain such subroutine. The area integrals involving the inertia terms in the dynamic J integral were less than three percent of the maximum J-integral values of the 7075-T6 and the 2024-T3 SEN specimens and thus the dynamic J and T^*_ε-integrals were reduced to their static counterparts. J-integral was computed along a square contour which remained fixed in size and moved with the crack tip. The T^*_ε-integral was computed along a contour, Γ_ε, which elongated with the moving crack tip. Only a near-crack contour, i.e. $\varepsilon = 2$ mm from the crack, was used in the integration process thus simplifying the T^*_ε computation by neglecting the contour integral behind the propagating crack .

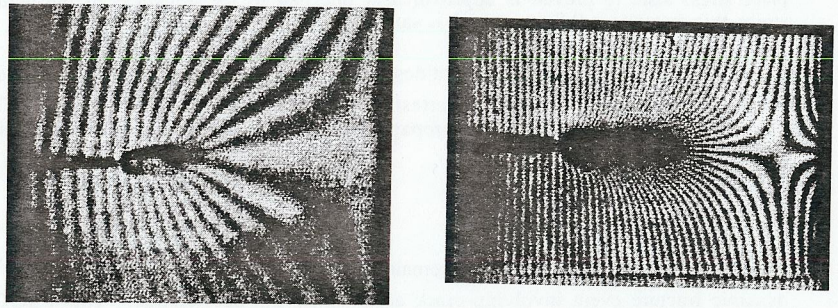

7075-T6 Specimen 2024-T3 Specimen

Figure 3. Dynamic Moiré Patterns of Fracturing Aluminum SEN Specimens.

RESULTS

Figure 3 shows typical dynamic Moiré fringe patterns associated with a propagating crack in 7075-T6 and 2024-T3 SEN specimens. While the crack in the 7075-T6 specimen accelerated to a crack velocity of 35 m/s, the crack in the 2024-T3 specimen gradually decelerated from a high of 5 m/s and arrested.

Figure 4 shows the variations of CTOA in the two specimens. The CTOA reached a steady state value after an initial high value similar to that observed by Dawicke et al (1995). The close matches between the computed and measured crack opening profiles in Figure 5 validated the FE modeling of the dynamic ductile fracture experiments. The crack opening profile retained the initial tip blunting prior to crack extension throughout the crack extension history.

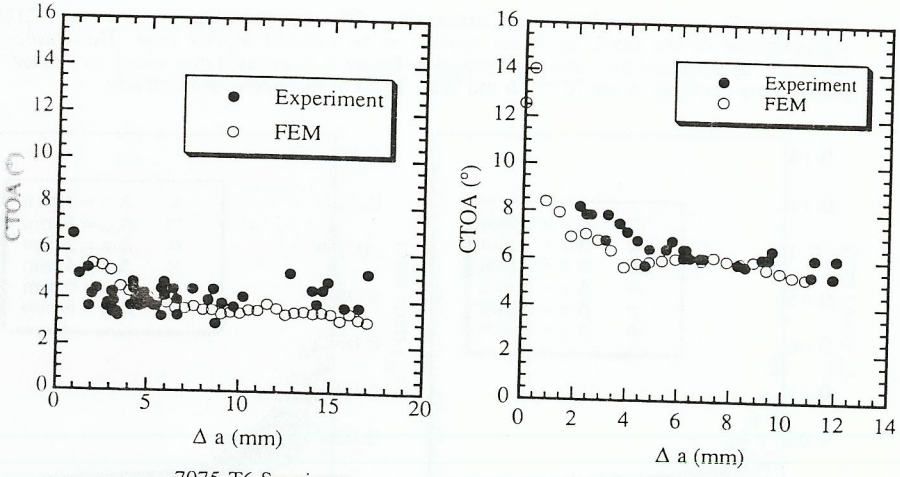

Figure 4. CTOA Variations With Rapid Crack Extension in Aluminum SEN Specimens.

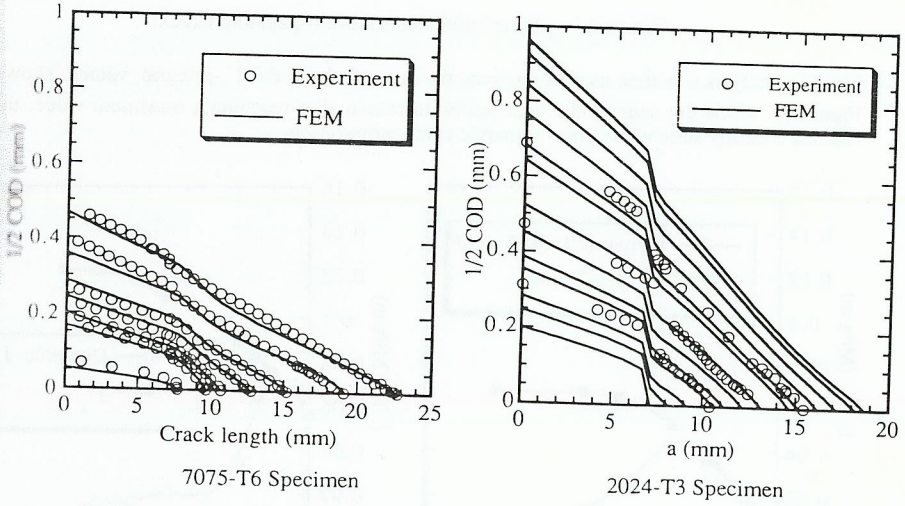

Figure 5. Variations in Crack Opening Profiles in Aluminum SEN Specimens.

The normal strain, ε_{yy}, distribution, which were obtained through FE analysis, ahead of the propagating crack are shown in Figure 6. Unlike the CTOA variation, ε_{yy} at the crack tip

continuously increased with crack extension. The common notion that the CTOA is representative of the crack tip strain appears to be violated in this case. The elastic-plastic boundary, as surmised from the yield strains in Figure 2, is nearly 4 mm and 8 mm ahead of the propagating crack tip in the 7075-T6 and 2024-T3 SEN specimens, respectively.

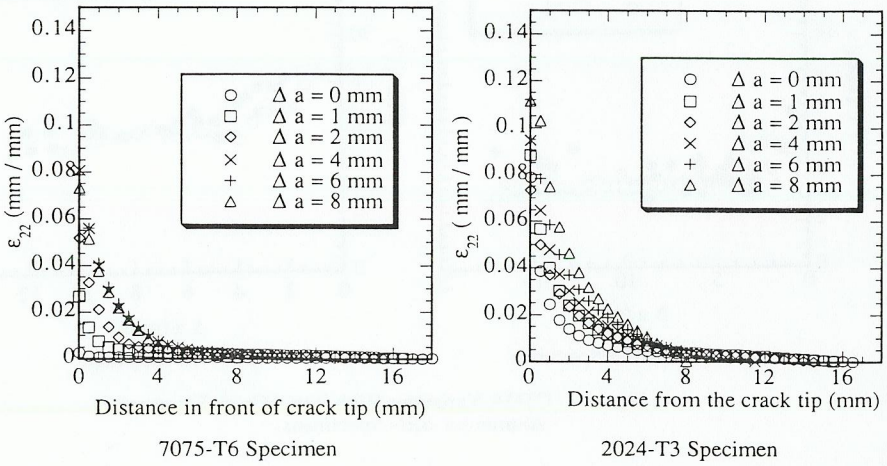

Figure 6. ε_{yy} Distribution Ahead of Propagating Crack.

The FE analysis was then used to compute the dynamic J and the T^*_ε-integral values shown in Figure 7. While the near field J continually decreased after reaching a maximum value, the T^*_ε reached a steady state value under dynamic crack propagation.

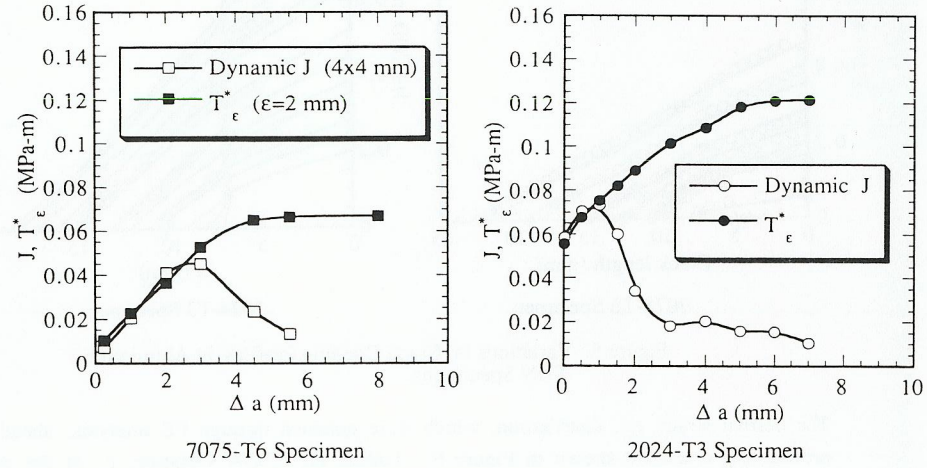

Figure 7. T^*_ε and J Variations in Aluminum SEN Specimens. ε = 2 mm.

DISCUSSIONS

Both the T^*_ε and CTOA are being considered for stable crack growth criterion and likewise conclusion could be reached for a dynamic ductile fracture criteria. CTOA, by definition, is a local crack tip parameter with a precipitous drop at the initial phase of rapid crack propagation. While Dawicke et al (1995) attribute this drop to crack front tunneling prior to crack extension, it has been duplicated by plane stress FE analysis without tunneling. Thus the initial drop in CTOA is probably due to crack tip blunting prior to crack extension. CTOA does not correlate directly with the state of FE strain ahead of the propagating crack as indicated by the increasing ε_{yy} at the extending crack tip in Figure 5. Moreover, recent unpublished results show that the CTOA appeared insensitive to thickness variation while T^*_ε decreased with doubling of the thickness of 2024-T3 aluminum specimens.

Since T^*_ε is evaluated a finite ε distance from the crack tip, it represent the thickness average of crack tip state despite the existence of 100 percent shear lip in both 7075-T6 and 2024-T3 specimens. Narasimhan and Rosakis (1990) have shown that the minimum distance for the plane stress state to prevail is approximately one half of the thickness of the plate. For this study, this distance is 0.8 mm which is satisfied here.

Both CTOA and T^*_ε remained constant despite the increasing velocity in 7075-T6 specimens and the decreasing and subsequent crack arrest in 2024-T3 specimens. Thus CTOA and T^*_ε could be the necessary condition for crack propagation with the condition for crack arrest yet to be determined.

CONCLUSIONS

Both the T^*_ε-integral and CTOA remained constant while J-integral diminished during the dynamic fracture event involving crack acceleration and deceleration. The T^*_ε/CTOA criteria proposed for stable crack growth could be the necessary condition for rapid crack propagation.

ACKNOWLEDGMENT

This study was supported by Office of Naval Research Contract N0001489J1276. The authors acknowledge the patience and encouragement of Dr. Y. D. S. Rajapakse, ONR during the difficult period of the experimental analysis.

REFERENCES

Brust, F. W., Nishioka, T., Atluri, S. N. and Nakagaki, M., (1985), "Further studies on elastic-plastic stable fracture utilizing the T^*-integral," *Engineering Fracture Mechanics*, vol. 22, pp. 1079-1103.

Dawicke, D. S., Sutton, M., Newman, J. C. and Bigelow, C.A., (1995), "Measurement and analysis of critical CTOA for thin-sheet aluminum alloy materials," *Fracture Mechanics, 25th Volume*, ed. F. Erdogan , ASTM STP 1220, pp. 358-379.

Kanninen, M. F. and Popelar, C. H., (1985), Chapter 4, "Dynamic fracture mechanics," *Advanced Fracture Mechanics*, pp. 192-280.

Kobayashi, A. S., Harris, D. O. and Engstrom, W. L., (1967a), "Transient analysis in a fracturing magnesium plate," *Experimental Mechanics*, vol. 7, No. 10, pp. 434-440.

Kobayashi, A. S. and Engstrom, W. L. (1967b), "Transient analysis in fracturing aluminum plates," *Proc. 1967 JSME Semi-International Symposium*, pp. 172-181.

May, G. B. and Kobayashi, A. S., 1995, "Plane stress stable crack growth and J-integral/HRR field," *Journal of Solids and Structures*, vol. 37, pp. 857-881.

Narasimhan, R. and Rosakis, A. J., (1990), "Three-dimensional effects near a crack tip in a ductile three-point bend specimen: Part I - A numerical investigation," *ASME J. of Applied Mechanics*, vol. 57, pp. 607-617.

Okada, H. and Atluri, S. N., "T^*_ε-integral evaluation from experimental displacement field for a plate with stably propagating crack: Development of calculation procedure and implication of T^*_ε," to be submitted.

Omori, Y., Okada, H., Ma. L., Atluri, S. N. and Kobayashi, A. S., (1996), "T^*_ε-integral under plane stress crack growth," to be published in *Fracture Mechanics, 27th Volume*, ASTM.

Stonesifer, R. C. and Atluri, S. N., (1982), "On the study of the $(\Delta \underline{T})_c$ and C^* integrals for fracture analysis under non- steady creep," *Engineering Fracture Mechanics*, vol. 16, No. 5, pp. 625-643.

Wang, F. X., May, G. B. and Kobayashi, A. S., (1994), "Low-spatial frequency steep geometric grating for use in Moiré interferometry," *Optical Engineering*, vol. 33, pp. 1125-1131.